University of Groningen

Titratable Martini model for constant pH simulations

Grünewald, Fabian; Souza, Paulo C T; Abdizadeh, Haleh; Barnoud, Jonathan; de Vries, Alex H; Marrink, Siewert J

IMPORTANT NOTE: You are advised to consult the publisher's version (publisher's PDF) if you wish to cite from it. Please check the document version below.

Document Version
Publisher's PDF, also known as Version of record

[Link to publication in University of Groningen/UMCG research database](#)

Titratable Martini model for constant pH simulations 🄵

Fabian Grünewald 🄳, Paulo C. T. Souza 🄳, Haleh Abdizadeh, Jonathan Barnoud 🄳, Alex H. de Vries 🄳, and Siewert J. Marrink 🄳

COLLECTIONS

Paper published as part of the special topic on Classical Molecular Dynamics (MD) Simulations: Codes, Algorithms, Force fields, and Applications

Note: This paper is part of the JCP Special Topic on Classical Molecular Dynamics (MD) Simulations: Codes, Algorithms, Force fields, and Applications.

🄵 This paper was selected as Featured

View Online   Export Citation   CrossMark

ARTICLES YOU MAY BE INTERESTED IN

Optimal estimates of self-diffusion coefficients from molecular dynamics simulations
The Journal of Chemical Physics **153**, 024116 (2020); https://doi.org/10.1063/5.0008312

Toward empirical force fields that match experimental observables
The Journal of Chemical Physics **152**, 230902 (2020); https://doi.org/10.1063/5.0011346

A well-behaved theoretical framework for ReaxFF reactive force fields
The Journal of Chemical Physics **153**, 021102 (2020); https://doi.org/10.1063/5.0013906

Titratable Martini model for constant pH simulations Ⓕ

View Online   Export Citation   CrossMark

Fabian Grünewald,[1] Ⓘ Paulo C. T. Souza,[1] Ⓘ Haleh Abdizadeh,[1] Jonathan Barnoud,[1,2] Ⓘ Alex H. de Vries,[1] Ⓘ and Siewert J. Marrink[1,a) Ⓘ

AFFILIATIONS

[1] Groningen Biomolecular Sciences and Biotechnology Institute and Zernike Institute for Advanced Materials,
 University of Groningen, Groningen, The Netherlands
[2] Intangible Realities Laboratory, School of Chemistry, University of Bristol, Bristol, United Kingdom

Note: This paper is part of the JCP Special Topic on Classical Molecular Dynamics (MD) Simulations: Codes, Algorithms, Force fields, and Applications.
[a)] Author to whom correspondence should be addressed: s.j.marrink@rug.nl

ABSTRACT

In this work, we deliver a proof of concept for a fast method that introduces pH effects into classical coarse-grained (CG) molecular dynamics simulations. Our approach is based upon the latest version of the popular Martini CG model to which explicit proton mimicking particles are added. We verify our approach against experimental data involving several different molecules and different environmental conditions. In particular, we compute titration curves, pH dependent free energies of transfer, and lipid bilayer membrane affinities as a function of pH. Using oleic acid as an example compound, we further illustrate that our method can be used to study passive translocation in lipid bilayers via protonation. Finally, our model reproduces qualitatively the expansion of the macromolecule dendrimer poly(propylene imine) as well as the associated pKa shift of its different generations. This example demonstrates that our model is able to pick up collective interactions between titratable sites in large molecules comprising many titratable functional groups.

Published under license by AIP Publishing. https://doi.org/10.1063/5.0014258

I. INTRODUCTION

Molecular Dynamics (MD) is a well-established method for simulating systems at molecular level. Depending on the time and length scales relevant for the specific system, either atomistic or coarse-grained (CG) models are used. One of the most commonly used CG models for (bio)-molecular simulations is the Martini model.[1] The Martini model has been successfully applied to many different areas in both molecular biology[2–4] and material science.[5–7] However, many technologically and biologically relevant processes are affected by the pH or pH gradients within a system of interest. Examples include translocation of drugs across membranes,[8,9] protein–protein interactions,[10,11] and response control of hydrogels.[12] A number of methods exist for introducing a constant pH in classical (i.e., non-reactive) atomistic simulations, such as the empirical-valence-bond approach,[13,14] the so called λ-dynamics approach,[15,16] and stochastic Monte-Carlo based approaches.[17,18] Recently, much effort is devoted to optimize the λ-dynamics

based methods in terms of the speed[19] and by introducing more physical details into the simulations[16,19–23] (e.g., long-range electrostatics or charge neutrality). However, until now, these methods are hardly applied to Martini-based systems[24] most likely because their slow-down that—at least until recently—is significant and voids the advantage of having a coarse-grained model in the first place. In addition, these methods require a somewhat lengthy procedure to parameterize and then to create the simulation engine dependent run setup. In fact, two of the most popular packages Martini is used with, namely, NAMD and GROMACS, were lacking an implementation for a long time. A native implementation in NAMD only recently has been released,[25] which currently does not support GPU acceleration. GROMACS is currently developing a constant pH support for their most recent versions, but it has not been published yet.

To efficiently capture the effects of pH in a simple manner that is consistent with the Martini spirit, here, we present a proof of

concept for an entirely different approach to constant pH simulations. In our method, protons are represented as explicit particles in the equations of motion and allowed hopping between CG water sites and titratable groups, both acids and bases. The relative affinity of the proton for a specific group is tuned to experimental titration curves and depends on the system's pH, which is set as the external variable. The number of titratable groups in the system is unlimited and naturally captures pKa shifts due to the local environment.

Our semi-quantitative approach is specifically optimized to work with the most recent Martini model, in principle, portable to all standard simulation engines, and allows for easy interpretation of pH related phenomena due to the use of an explicit proton particle. Thus, we aim to extend the scope of the current constant pH methodologies and benefit from the large speed up of CG over common atomistic simulations.

The rest of the paper is organized as follows: First, we present the new constant pH method and the parameterization process. Subsequently, we present selected examples demonstrating the validity of our approach, followed by a brief discussion on the limitations and future perspective of the model.

II. THE MODEL

A. The concept

The titratable Martini model is an extension of the latest version (3.0) of the Martini model. In the Martini force field,[1] two to five non-hydrogen atoms are grouped, with their connected hydrogen atoms, into one interaction center, called a bead. The interactions between beads represent the nature of the underlying chemical groups; the strength of the interaction is selected from a discrete set of Lennard-Jones (LJ) interactions by reproducing thermodynamic data, mostly the free energies of transfer between water and different organic solvents as well as solvent miscibility. Particles carrying charges further interact through a Coulomb potential. In addition to the regular Martini beads, smaller bead sizes (S- and T-beads) are used for groups that are represented at a higher resolution such as aromatic rings.

Here, we introduce a new class of Martini beads, the so-called titratable beads, that have the ability to change their protonation state as a consequence of a change of the environment or the pH. The key difference between titratable and regular beads is that titratable ones can reversibly bind a positive particle called a proton bead (Fig. 1). From an interpretive point of view, one can consider the proton bead to be a proton. Note, however, that we do not aim to model a real proton, but rather to capture the effect of proton transfer. The "proton bead" should thus be interpreted as an effective carrier of chemical information transferred during a (de)protonation event. Not only the titratable beads can bind to a proton bead but also every water bead can donate or accept such a bead, thereby providing a reservoir of available proton beads in the direct environment of the titratable groups. Our titratable water model represents on average four water molecules as one particle following the tradition of previous Martini models. Earlier, Yesylevskyy,[26] Wu,[27] and Michalowsky[28] and their respective co-workers parameterized a polarizable Martini water model, with a negative and
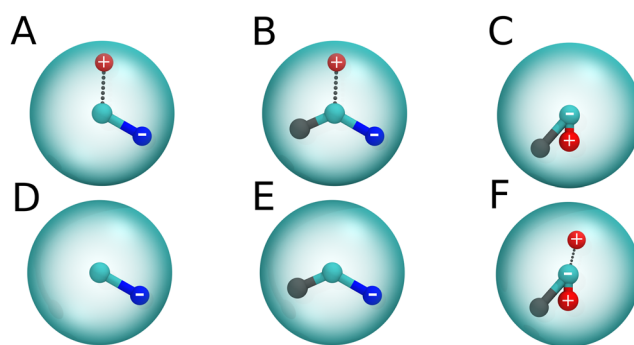

FIG. 1. Titratable Martini bead geometries. The upper row shows the internal geometry for the neutral species of water (a), acids (b), and bases (c). The lower row shows the charged versions in matching order. Red particles connected by dots representing the non-bonded attraction are proton beads. Red particles connected by a bond are dummy particles as are the gray and blue particles. These dummy particles only interact with protons and titratable beads, while cyan particles are the central interaction sites. All charged dummy particles also interact with charged beads.

positive dummy charge offset from the LJ center to mimic polarization effects. We utilize this type of internal bead geometry for our titratable water model as well. Note that from here onwards, we define the term dummy to describe particles that do not represent a specific chemical fragment. They rather help in the description of the underlying fragment and, for example, provide polarization or directional interaction with the proton bead. Such dummy particles only interact with charged particles, the proton bead, and each other. Whereas the negative dummy particle is retained as in the previous polarizable models, in the titratable model, the positive charge (i.e. proton bead) is reversibly attached to the water bead by a LJ interaction to the central interaction site. Thus, each Martini water particle can accept and donate a proton bead [see Figs. 1(a) and 1(d)]. This enables proton beads to transfer between water sites in a hopping like process reminiscent of the Grotthuss mechanism[29] in real water. Ironically, an excess proton on a CG water bead (i.e., per four water molecules) is reminiscent of an Eigen cluster ($H_9O_4^+$).[30]

Other titratable beads representing acids or bases follow the same basic principle as the water model. They internally have a set of dummy particles and can reversibly bind a proton bead [Figs. 1(b) and 1(c)]. The central interaction site mediates all LJ interactions with neutral and non-titratable beads. The geometries of the dummy sites are generic for acids and bases, respectively. Therefore, they are independent of the underlying fragment and used for all beads of either category. We utilize three major types of dummy particles for acids, bases, and water, as shown in Fig. 1. Both acids and water have a dummy particle that carries a negative charge displaced from the center, whereas for the bases, the negative charge is located at the center. Shifting the charge is essential in creating a higher proton affinity for bases. In addition, both bases and acids have neutral dummy particles (gray in Fig. 1) that we found beneficial in preventing excess protonation, which can, in principle, happen because our beads are rotationally isotropic. Thus, a proton can bind from all directions. In contrast, proton binding in reality is largely anisotropic. Apart from a slightly different internal geometry, we

distinguish acids and bases based on the following rule: Acids lose a proton bead going from the neutral [Fig. 1(b)] to the charged state [Fig. 1(e)], whereas bases accept a proton bead in going from the neutral [Fig. 1(c)] to the charged state [Fig. 1(f)]. Hence, a protonated acid is charge neutral, while a protonated base is positively charged, which mimics the Arrhenius definition for acids and bases. Using this concept of a proton bead, one can simulate titrations with Martini. For example, a base in titratable Martini water will accept a positive particle when the pH is below the pKa. The free energy ($\Delta G_{prot.}$) of this process depends on the pH and the pKa of a given group,[15]

$$\Delta G_{prot.} = RT \times \log(10) \times (pKa - pH). \tag{1}$$

According to Eq. (1), the probability of protonation, which is proportional to the free energy, increases with the decrease in pH. The origin of this increased probability is related to the increased concentration of hydronium ions. Thus, in an explicit particle approach to pH, one could try to model the pH effect by simply increasing the concentration of the excess protons. However, dealing with constant concentrations in simulations is impractical, especially around physiological pH where the excess proton concentration is of the order of 10^{-7} mol/l. Equilibration will be slow and requires removal or addition of particles in the course of the simulation when protonation states change. In addition, proton concentrations in heterogeneous systems—for instance, close to a membrane—are not always well defined. To circumvent these kinds of problems and get the benefits of an explicit particle approach, we apply a simple inversion of reasoning: As in a real system, in our simulation, every titratable Martini water bead can accept or donate a proton. To change the probability of protonation of an acid/base as a consequence of pH changes, we increase the availability of proton beads instead of their concentration. The availability is increased by lowering the proton bead interaction with the water beads. In this fashion, we modulate the degree of protonation of an acid/base and the associated free energy. At the same time, the total concentration of positive dummy particles remains constant, and the solution charge is neutral. To implement this concept, we introduce a set of interactions that are pH dependent and that are fixed at the start of the simulation. Because our titratable model builds on top of the Martini model, we utilize the same non-bonded interaction functions (i.e., Lennard-Jones and Coulomb potentials). This compatibility allows us to retain all parameters for the neutral Martini beads; we only parameterize pH dependent water models (Sec. II B) and introduce a new class of titratable beads (Sec. II C). An exception forms the class of charged Martini beads, which need an adjustment when using titratable Martini as the dielectric screening constant of the titratable water model is different from the value used before (Sec. II D).

B. Parameterization of titratable martini water

As discussed in Sec. II A, the affinity of water for the proton bead changes as a function of pH. The pH scale corresponds to a regular spacing of the LJ well depth between the proton bead and central site from ε = 1.0 kJ/mol to ε = 34.34 kJ/mol. The upper limit is determined by stability of the simulation. Above 35 kJ/mol, the simulation becomes numerically unstable using a 8 fs–10 fs time step, which we consider as a lower limit for efficient

integration of the equations of motion for the Martini model. We have further defined that the lowest interaction parameter corresponds to pH 3.0 and the highest to pH 8.0. Whereas it would be optimal to span a pH range between 0 and 14, for most biomolecular systems, a pH range of 3–8 is sufficiently wide to simulate many pH dependent processes. The negative dummy particle on water and any other charged bead has a small repulsive LJ potential with respect to the proton to prevent the charges from overlapping. All GROMACS input files and the parameters for these models can be found online (https://www.cgmartini.nl) and in the supplementary material.

The self-interaction of the water bead needs to be changed as a function of pH as well. With the decrease in pH (i.e., proton affinity), the effective water–water interaction decreases as well. In order to keep the density of water reasonable, we increase the water–water interactions through adjustment of the LJ interactions between the central interaction sites. To make it fully compatible with neutral beads of Martini, we adjusted the water self-interaction such that the solvation free energy of neutral beads is the same as in Martini (version 3.0) at every pH. In this manner, all free energies of transfer of the neutral beads to the aqueous phase are accurate without further adjustment. The price to pay for this match is that the density of the water model changes slightly as a function of pH. The lowest density (955.7 kg/cm^3) is observed at pH 3.0, and the highest density (1017.08 kg/cm^3) at pH 8.0. They correspond to 4.2% and 2% deviation from the experiment, which for a coarse-grained model is very acceptable. Further validation of the titratable water model is provided in the supplementary material.

C. Titratable acids and bases

Martini beads are divided into four major categories ranging from apolar via neutral to polar and charged beads. Within the titratable model, the polar and neutral beads can, in principle, become titratable, if they are meant to represent an acid or a base. Water is always titratable. As in regular Martini, the titratable version of a bead represents a molecular fragment; this fragment can be used in different molecules in the spirit of the building block approach. For establishing a proof of concept, we have generated parameters for a number of acid and base fragments and more complex molecules that include these fragments. Nevertheless, the protocol is essentially transferable such that any acid or base could be simulated. As discussed previously, each titratable bead has an internal geometry of charged or neutral dummy particles that facilitate proton binding. However, the central interaction site has a LJ interaction with the proton bead as well. This LJ interaction can be tuned to set the degree of deprotonation (α) according to the pKa. Both the sigma and epsilon value of this interaction were adjusted to reproduce the experimental pKa value and the titration curves of the underlying fragments as well as possible. The pKa values are obtained by fitting the degree of deprotonation as function of pH to the following equation:

$$\alpha = \frac{1}{10^{q \times (pH - pKa)} + 1}. \tag{2}$$

In contrast to the other constant pH methods,[15,16] we add a factor q that captures deviations from perfect dilute solution behavior.

Usually q, also called the Hill coefficient, measures the cooperativity between multiple titratable sites. In a strict sense, q should be 1 for a single titratable site in dilute solution [the case in which Eq. (2) reduces to the well-known Henderson–Hasselbalch equation], and its variation in the presence of other sites describes the degree of cooperativity between them. However, due to inherent limitations of our approach (discussed in Sec. III A), we cannot reproduce perfect titration behavior. Therefore, in the spirit of a semi quantitative method, we use the q factor as a measure to compare deviations in titration behavior to the reference titration curves. As detailed in Sec. III D, we are still able to qualitatively and, to some extent, quantitatively capture cooperativity in complex systems despite q deviating from 1 for acids/bases in dilute solution.

The pKa of the target compound also appears in the naming of the bead. For example, an acid bead representing acetic acid (pKa = 4.76[31]) would be P2_4.8. In general, we consider that a titratable bead can be used for the same fragment in any molecule, if the pKa is not too different. As the proton bead does not interact with neutral non-titratable beads, a titratable bead behaves like its non-titratable counterpart in any organic solvent. Because these interactions are defined in the standard Martini force field, we did not have to reparameterize these interactions with the other beads. Interactions with the aqueous solvent, however, are significantly different between the standard and titratable water models and required recalibration. To recalibrate these LJ interactions, we adjusted the epsilon value to reproduce the free energy of transfer between organic solvents and water for the reference fragment. Because acids and bases can change their ionization state when transferring into another solvent, we use the distribution coefficient, log(D), instead of the partition coefficient, log(P), to compute the free energy of transfer [Eq. (3)]. The distribution coefficient can easily be obtained from the partition coefficient of the neutral species by adding a pH dependent term [Eq. (4)],[32]

$$\Delta G_{transf.} = -RT \times \log(10) \times \log(D), \qquad (3)$$

$$\log(D) = \begin{cases} \log(P) + \log\left(1 + 10^{q(pKa-pH)}\right) acid \\ \log(P) + \log\left(1 + 10^{q(pH-pKa)}\right) base \end{cases} . \qquad (4)$$

As we will explain when discussing the free energies of transfer, the water titratable bead interaction is also pH dependent. This corrects for a mismatch of our titration curves with the theoretically perfect titration curves. Once the water interaction is optimized, the single beads can be combined with any other fragment to represent a more complex molecule, in principle, without adjustment. However, for the primary amines with pKa values larger than 8, we noticed that the free energy of transfer is only accurately reproduced for such compounds after applying a shift in the water interaction. Thus, we need to distinguish whether the amine is free or bound to something else, but not which compound it is part of exactly.

To summarize, a titratable Martini acid/base bead is based on two components: the proton interaction reflecting the pKa and the remaining interactions reflecting the hydrophilicity of the fragment. To assign an optimal bead type for a given acid or base, one selects the neutral bead that fits the neutral species the best and subsequently selects the titratable bead of the same type with the best

matching pKa. The specific model parameters can be found in the supplementary material and online (https://www.cgmartini.nl).

D. Readjusting charged beads

Only ions represented by single beads and dummy particles of the titratable beads carry a charge in our model. The ions follow the same classification as in Martini 3. However, because the dielectric constant of the titratable model differs from the standard value (see Sec. II E), the parameters of those beads need to be readjusted, similar to what was done in the case of the polarizable water model.[26] For the proof of principle, we only include normal sized ions of the types corresponding to the head-group of the phosphocholine lipids and hydrated sodium/chloride. Their interactions are optimized to match lipid bilayer properties of Martini 3 such as area per lipid. Likewise, the ions need to be repulsive with respect to the oppositely charged interaction sites in the water and acid/base beads to avoid the charge catastrophe from overlapping charged beads. A simple repulsive LJ interaction is applied that is not further optimized.

E. Essential simulation parameters

Following the standard practice for simulations with the Martini model,[33] the van der Waals non-bonded interactions are cut off at 1.1 nm using the respective Verlet-shift-modifier for LJ interactions. We use the Verlet neighbor list scheme with the default update of the neighbor list of 10 steps and a Verlet-buffer tolerance of 0.005 kJ/mol/ps. Benefitting from the explicit dielectric screening of the titratable water model, Particle Mesh Ewald (PME) summation is applied to capture the long-range electrostatics. In addition, the titratable model uses a system-wide dielectric constant of 6 for implicit screening. Alternatively, we could have also scaled the charges as done previously in the polarizable water models.[26,28] However, we considered it more appropriate to retain the proton with a plus 1 charge. Clearly, a dielectric constant 6 is too high for alkanes and too low for water. However, since our water is protonatable and in that sense polarizable, we recover some electrostatic screening. Any necessary energy differences arising from a different dielectric constant that are not captured by this polarization will implicitly become part of the LJ interaction of acids, bases, and ions. It should be noted that these parameters are part of the model and should not be changed without verification.

III. RESULTS AND DISCUSSION

A. Reproducing titration curves

The proton affinity of an acid/base bead is adjusted to reproduce the titration curves of a given pKa. Figure 2 shows a set of titration curves for selected acids and bases. It shows that we can qualitatively reproduce the titration curves of a diverse range of common acids and bases, thereby capturing essential features of them. For example, the degree of de-protonation of acetic acid is about 1 starting from pH values close to 7 and drops below 20% at low pH, meaning that it is mostly protonated. At around the pKa (4.76[31]), we observe the largest change in the degree of protonation as would be expected from the real system. Similar trends are observed for the
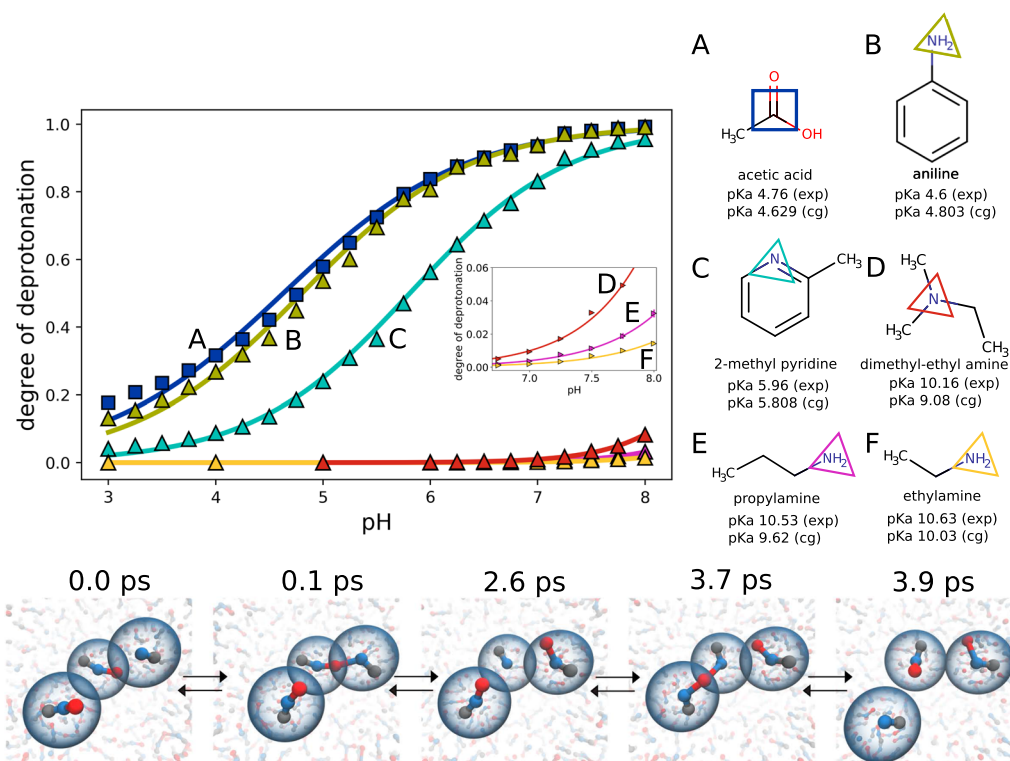
FIG. 2. Acid/base titration with Martini. Upper panel: titration curves of six model compounds and their chemical structure (A-F) as well as the corresponding pKas from simulation and experiment. Solid lines are fits to the simulation data using Eq. (2). Note that the error of individual data points is smaller than the symbol width and generally in the order of 0.01. The titratable residue is indicated by squares in the case of an acid and triangles in the case of a base in the chemical structure. The experimental pKa values are taken from the literature.[31,34–36] The lower panel shows a consecutive proton transfer from water to another water and subsequently abstraction of a proton by the ionized water from another water in a hopping-like fashion. A video of this process is shown in the supplementary material.

base 2-methyl pyridine (pKa = 5.96[34]) or aniline, which both change from ionized to neutral over the pH range 3–8. To some extent, we also capture the behavior of stronger bases such as ethyl-amine (pKa = 10.63[35]). In high pKa cases, the molecule is mostly ionized over the entire pH range, and only toward pH 8.0, a slight increase in the degree of deprotonation is observed. We note that the protonation curves deviate somewhat from a perfect sigmoidal shape (e.g., compare Fig. S2). Especially for acetic-acid and diclofenac, the titration curves are less steep and retain a higher degree of deprotonation at lower pHs.

We attribute the deviations in the degree of deprotonation to the approximate potential for proton binding and the isotropic nature of a single CG bead as opposed to the underlying anisotropic acid/base fragment it represents. In particular, small acids or bases that are represented as a single titratable bead (e.g., acetic acid) are rotationally isotropic at the CG level and therefore capable of binding a proton also to the side that would be naturally excluded in the real compound. This is to some extent recovered by the additional dummy site, but not fully. As a consequence, the proton interaction has to be a compromise between avoiding excessive over protonation at low pH and still being largely deprotonated at high pH, with maximum curvature around the pKa. In all cases, including

the strong bases, the protonation state is rather dynamic; protons exchange over time as they do in our water model (and in reality). As shown in Fig. 2, a proton can hop from water to another water protonating it, and subsequently, the ionized water can get a proton from its neighboring water in a hopping kind of fashion. The typical time scale of these events is in the ps up to 1 ns range. A video of waters exchanging protons is available in the supplementary material. Our proton diffusion rate D^{prot} is the fastest at pH 3.0 ($D^{prot} = 4.1 \pm 0.4 \times 10^{-5}$ cm$^2 \times$ s^{-1}) with an average residence time of ~22 ps. The slowest diffusion is observed at pH 8.0 ($D^{prot} = 0.8 \pm 0.4 \times 10^{-5}$ cm$^2 \times$ s^{-1}) with a residence time of 400 ps. This dynamic and fast proton diffusion allows for a fast equilibration of acid/base protonation states. Our water model also captures the experimentally measured effect of faster proton diffusion relative to water.[37,38] A small discussion on the water diffusion can be found in the supplementary material. As compared in Fig. 2 and Table S4, we can utilize these acid/base building blocks in the Martini spirit to generate more complex molecules while retaining a realistic pKa value. For the strong primary amines, deviations of the pKa are in the order of 1.0 pKa units, but the qualitative ordering in the degree of protonation is preserved. In most other cases, experimental pKa values can be reproduced to within 0.5 pKa unit.

We consider such deviation units acceptable, as this corresponds to a deviation of the order of RT in the free energy of protonation. Thus, from a protonation perspective, the titratable beads are transferable.

B. Reproducing pH dependent transfer free energies

In Sec. III A, we showed that our titratable beads reproduce the titration curves of acids/bases with different pKas and display dynamic protonation equilibria. However, we also need to assure that the titratable beads show correct trends in partitioning between different environments, one of the corner stones of the Martini model. Because acids and bases can change their ionization state when transferring into another solvent, we use the distribution coefficient, log(D), instead of the partition coefficient, log(P), to validate their behavior. Inspecting Eq. (3) more closely, we see that the pH dependent part contains the protonation free energy [cf. Eq. (1)]. For example, if for an acid, the pKa is smaller than the pH, we can drop the 1 from the log and retain the protonation free energy. We therefore can interpret this free energy as the process of taking the acid/base at some pH, then protonating it, and subsequently transferring it into the organic phase. Figure 3(a) shows the corresponding PMFs for such a process for acetic acid at several pH values. At pH values of 3.0, 4.0, and 4.5 (i.e., below the pKa), the free energy of protonation is about zero and the free energy of transfer is just that of the neutral species. However, at pH values larger than the pKa, there is a free energy penalty to abstract a proton and go into the oil phase. This leads to an increase in the free energy of transfer. In principle, there could also be a contribution of the ionic species to the distribution coefficient and free energy of transfer.

For example, in a biphasic water–octanol system, there is a substantial amount of water present in the octanol phase, which can stabilize the ionic species.[41] However, for hexadecane, we can safely assume partitioning of the ionized species to be negligible. Thus, we parameterized all interactions based on hexadecane free energies of transfer to avoid problems of ionic species partitioning. After matching the free energy of transfer from water to hexadecane for our reference compounds, we computed the free energy of transfer at three pH values (3.0, 5.5, and 7.5) for several more complex molecules that have a single ionizable site. Figure 3(b) shows the correlation between the experimental and simulated values. The

full data can be found in Table S5. In general, we see a very good correlation with the experimental reference data across all pH values (R^2 = 0.98). The mean absolute error across all pHs and all species is 1.75 kJ/mol, whereby pH 7.5 has the highest absolute error (2.0 kJ/mol) and pH 5.5 has the lowest absolute error (1.13 kJ/mol). The overall match is very good, demonstrating that our titratable beads are not only transferable with respect to pKa but also with respect to the free energies of transfer. Thus, one can use, for example, the fragment based on acetic acid in all molecules with acetic acid fragments of similar pKa without the need to readjust any parameters.

C. Capturing pH dependent drug-membrane binding

Membrane binding affinities are an important measure to assess the environmental impact and toxicity of small molecule chemicals as well as drugs.[34] Although octanol–water partition coefficients are reliably correlated with membrane affinity, they are less reliable for ionizable compounds requiring more difficult measurements with real membranes,[42] columns,[34] or prediction with mechanistic modeling approaches.[43]

In this section, we demonstrate that, combining titratable beads with standard Martini beads, we are able to reproduce pH dependent bilayer affinities of a variety of compounds. We modeled a set of 8 compounds (see Table S7), 3 of which bear a carboxylic acid moiety and 5 of which are amine containing bases. The strongest change in bilayer affinities is seen for those compounds that change from neutral to ionized over the pH range we consider. Figure 4(a) shows the potential of mean force (PMF) of membrane binding as a function of distance from the center of the bilayer for 5-phenylvaleric acid (PVA) (red curves) and aniline (blue curves). At pH 3.0 (solid curves), PVA is neutral and has a larger membrane affinity than aniline, which is charged at this pH. The corresponding experimental membrane affinities of −18.1 kJ/mol[42] and −5.1 kJ/mol,[36] respectively, are in qualitative agreement with the ones obtained for our titratable model (−17.9 ± 0.3 kJ/mol and 0.3 ± 0.2 kJ/mol, respectively).

When increasing the pH to 7.5, PVA exists largely in ionic form and aniline as neutral species. This leads to a decrease in the membrane binding free energy of PVA and an increase in the membrane binding free energy of aniline. This antisymmetric trend is in qualitative agreement with the experimental observations, available
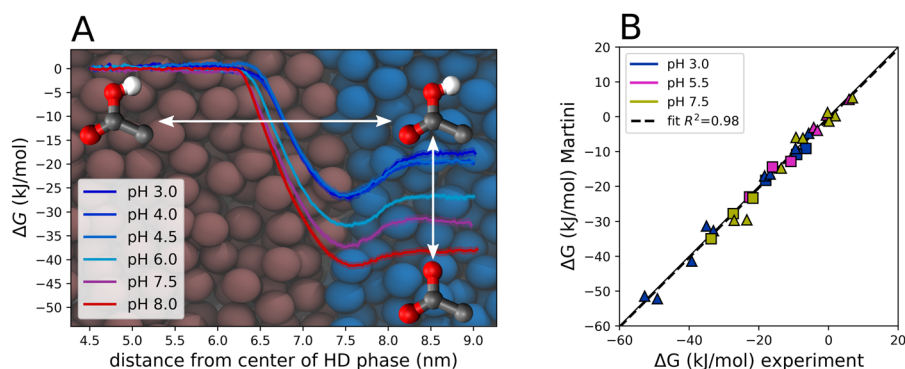
FIG. 3. pH dependent transfer free energies. (a) PMFs for the transfer of acetic acid into hexadecane (HD) at different pH values. (b) Correlation between free energies of transfer from hexadecane to water for acids (squares) and bases (triangles) in our titratable Martini model and experiment at three selected pH values: 3 (blue), 5.5 (pink), and 7.5 (gold). See Table S5 for data points. Experimental values are computed from pKas and neutral molecule partition coefficients, which were taken from Refs. 39 and 40.

FIG. 4. Drug-membrane interactions. (a) Potential of mean force (PMF) curves for 5-phenylvaleric acid (PVA, blue lines) and aniline (red lines) at two different pH values. PMFs at pH 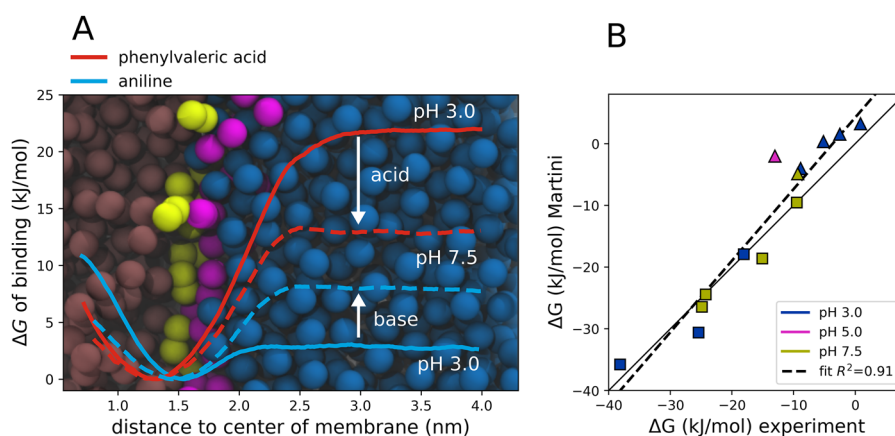3.0 are solid lines and PMFs at pH 7.5 are dashed lines. As a function of increasing the pH, the membrane affinity for the acid PVA decreases, whereas the affinity for the base aniline increases. These changes are generally expected for acids and bases.[42] (b) Correlation graph for membrane affinities of several other compounds at different pH values. Full data are given in Table S7 and experimental reference data taken from the literature.[34,36,42,44,45] Note that the x-axis for the PMF profiles in panel A is scaled to account for the different bilayer thicknesses at different pHs.

for some acids and bases.[42] At pH 7.5, the experimental membrane binding affinity of PVA is −9.47 kJ/mol[42] again in good agreement with our model, which gives a membrane affinity of −9.5 ± 0.3 kJ/mol. Whereas the agreement between the experimental membrane affinity (−9.3 kJ/mol[36]) and the one obtained using our model (−4.88 ± 0.04 kJ/mol) is less good for aniline, the difference in binding affinities between pH 3 and pH 7.5 (i.e. ΔΔG) is well reproduced for both PVA and aniline. This observation holds for all compounds for which data are available at two pH values (see Table S7). The mean absolute error in the ΔΔG of binding is 1.0 kJ/mol, with the largest deviation observed for myristic acid. That deviation is close to RT with 2.7 kJ/mol, which is still a good match. Overall, this example demonstrates that our model is able to qualitatively describe pH dependent membrane association processes. Figure 4(b) shows a correlation plot of experimental and simulated membrane affinities at different pH values. Our membrane affinities correlate well for both acids and bases across all pH values investigated, with a correlation coefficient of 0.91. Quantitatively, the model leaves room for improvement, with the mean absolute error in ΔG of about 3.48 kJ/mol. However, it is worth setting the error into perspective. Prediction of membrane affinities especially for ionic compounds is difficult, even for mechanistic procedures optimized for this purpose.[43] Our dataset contains 9 ionic compounds and 4 neutral ones.

Although one should be cautious when directly comparing these values, because our dataset is very small, it shows that even the quantitative performance is very promising at this stage. To summarize, our model can clearly capture trends and even some quantitative effects of membrane affinity of titratable molecules as a function of pH. On one hand, this validates that our titratable beads can be used in combination with Martini membranes. On the other hand, it shows that our method could be competitive to predict membrane affinities not only for neutral and charged species but also as a function of pH.

D. Capturing environment dependent pKa shifts

Capturing changes in the apparent pKa due to interactions with the environment is one of the most important aspects of any constant pH simulation methodology. In this section, we show that our model qualitatively captures such effects for two example cases. First, we discuss pKa shifts of oleic acids when present in a lipid membrane that constitutes a more hydrophobic environment. Subsequently, we discuss how the interaction between amines in poly(propylene imine) dendrimers results in pKa shifts and causes conformational changes as a function of pH.

It is well established that fatty acids bound to lipid bilayers have a shift of their pKa.[46] Figure 5(a) shows the titration curves for oleic acid bound to a POPC membrane in comparison to free oleic acid in solution as obtained with our titratable Martini model. Clearly, we observe a shift in the degree of protonation toward higher pKa values. Fitting the curves to Eq. (2) yield a pKa value of about 5.29 for the membrane bound acid vs 4.62 in aqueous solution. Although the precise values depend on the measurement techniques as well as on the bilayer, there seems to be agreement that the expected range of the shift should be between 1.5 and 2.0 pKa units.[46–48] Our model qualitatively captures this change, with a pKa shift of about 0.7 pKa unit. Protonation at the membrane interface is also crucial for the translocation process of fatty acids. Fatty acids can translocate the bilayer in neutral form at much higher rates than in the ionized form.[49,50] In our simulation, we observe rapid flip-flop of oleic acid in POPC at pH 3.0. At pH3, we observed 22 flip-flop events in 3 μs of simulation. As expected, increasing the pH leads to fewer flip-flop events in the same duration of simulation (Table S6). Flip-flop proceeds, in general, via the protonated form even at higher pH values (e.g., pH 6.0), where most of the acid is deprotonated. The flip-flop process at pH 6.0 is illustrated in Fig. 5(b) and shown in the video in the supplementary material.
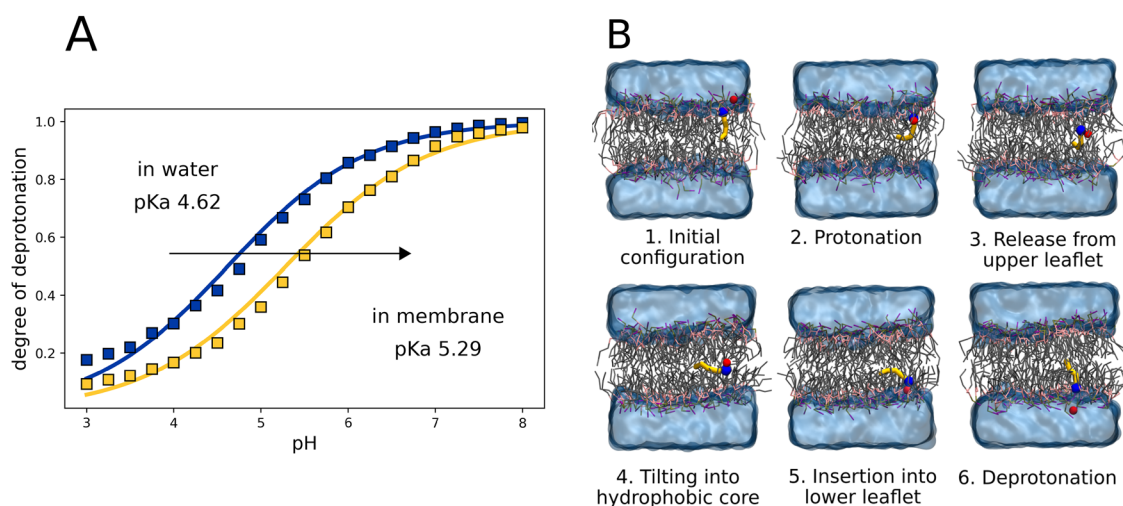
FIG. 5. Hydrophobic environment causes a shift in pKa. (a) Titration curve of oleic acid in water (blue) and POPC bilayer (yellow) showing a clear shift in the pKa value from 4.62 to 5.29. (b) Snapshots of a typical translocation event of oleic acid through a POPC bilayer. Initially, the oleic acid is deprotonated (1). After absorbing a proton from solution (2), the now neutral oleic acid dissolves into the membrane interior and flip-flops to the other side (3–5). Eventually, the oleic acid becomes deprotonated again (6). Lipid tails are shown in gray, the linker in pink, choline bead in purple, phosphate bead dark green, oleic acid in orange, and the titratable bead in blue, whereas the proton is shown in red. A video of the flip-flop process is available in the supplementary material.

In the long term, we aim at extending our methodology to complex proteins and biopolymers. However, to test, if our model shows any cooperativity between titratable sites, we simulated the titration of the G5 dendrimer poly(propylene imine) (PPI). PPI consists exclusively of primary and tertiary amines. Simulation of the titration reveals that the dendrimer expands with the decrease in pH. Figure 6 shows the radius of gyration for three pH values as well as the degree of protonation of each titratable site. Unfortunately, to our knowledge, no experimental study has investigated the expansion as a function of pH, but we can compare the expansion of about 0.31 nm–0.4 nm measured in atomistic simulations.[51] The increase in size of the molecule correlates well with the increased amount of protonated residues. At pH 7.5, only the outer amines are protonated. At this pH, the radius of gyration is the smallest. Decreasing the pH from 7.5 over 5.5, the inner amines become more protonated. At pH 3.0, all amines are protonated and the dendrimer fully expands. The total protonation level is in good agreement with the experimentally measured protonation state. Experimental data[52]

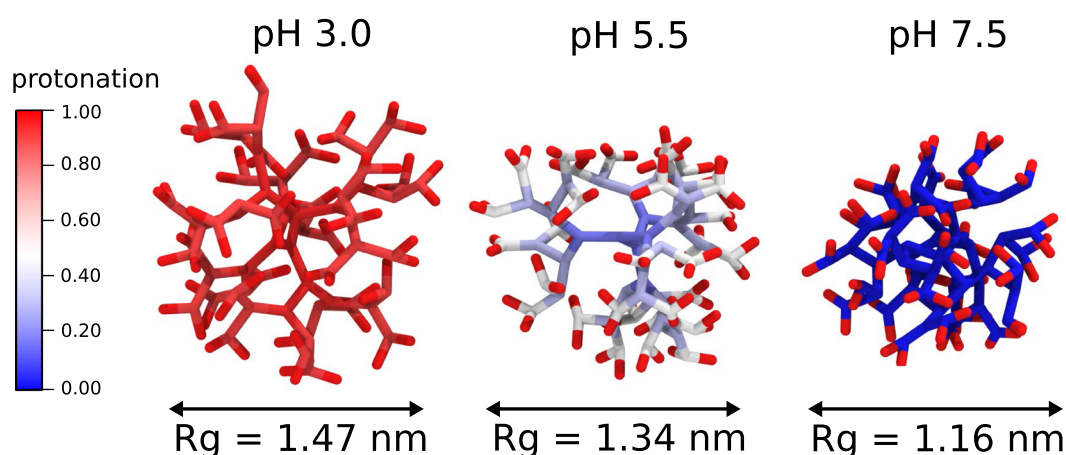**FIG. 6**. Cooperative titration of dendrimer bases. Snapshots of the simulated poly(propylene imine) (PPI) dendrimer are shown as a function of pH. The color range, from red (protonated most of the time) to blue (deprotonated most of the time), indicates the change in protonation of the bases. Due to the decreased charge density at higher pH, the polymer collapses as quantified by the radius of gyration (Rg).

indicate that at pH 3.0, the dendrimer is fully protonated, as in the simulation [cf. Figure 6(a)]. At pH 5.5 and 7.5, the deviations are somewhat larger with 83% and 63% protonation in the simulation compared to 72% and 51% in experiment. Figure S4 compares the total titration curves for more values of the pH range. Overall, we predict the total charge within 12% from experiment, which is very satisfactory. In addition, we resolve the approximate shape of two plateaus seen in the total titration curve. We proceeded to fit the titration data of the different generations (1–5) and obtained a microscopic pKa value.

Figure S5 in the supplementary material shows the fits and resulting pKa values. The highest pKa is found for the terminal amines (pKa 9.65 ± 0.05), which is almost unchanged with respect to the monomer pKa. One can therefore assume that the terminal amines are separated far enough so that cooperative effects are weak. However, moving into the dendrimer core, the pKa increases with each generation. That means the tendency to protonate decreases, with the innermost generation having a pKa of 5.00 ± 0.05. That is a shift by about 4 pKa units from the free solution pKa. To our knowledge, the pKa values have not been determined experimentally; however, our results are qualitatively consistent with those obtained for PAMAM dendrimers by titratable atomistic simulations.[53]

E. Limitations and future outlook

Although we have demonstrated above that our titratable Martini model can be used in a variety of different contexts and reproduce at least qualitatively experimental observations, some general and specific limitations still apply. In this section, we shall discuss these limitations to caution the users when applying the model. We will also point toward future improvements.

The titration curves for single acids/bases in solution are somewhat stretched with respect to the HH behavior. Specifically, we observe a higher percentage of deprotonated species for pH values lower than the pKa and a smaller percentage of deprotonated species for pH values higher than the pKa. A direct consequence of this behavior is that our reference titration curves (i.e., representing infinite dilution) have a non-zero Hill coefficient. Therefore, cooperativity can only be measured qualitatively in terms of the shift of the Hill coefficient in comparison to the reference state. We anticipate that in the future versions of our titratable Martini model, the empirical potential can be optimized to improve the titration curves. In particular, introducing an angle dependency of proton binding through either differently sized dummy beads or plainly through a bonded potential acting on the dummy beads would be possible solutions.

Specific dipole interactions with polar and hydrogen bond forming beads, which represent non-titratable groups, are not yet part of the model. In the current Martini model, when a group is a hydrogen bond donor or acceptor, a label is added, which modifies the interactions with other acceptor or donor beads. These labels account for hydrogen bonding that is not explicitly part of the model. Likewise, other labels can be added to account for strong dipole interactions. At the moment, titratable beads retain the label from the neutral bead. This missing interaction may account for the less strong pKa shift observed for the fatty acids in comparison to experimental estimates. Another consequence is that we cannot

compute octanol water free energies of transfer at the moment. It is known that octanol stabilizes small water micelles that allow ionic species to partition into octanol.[41] As we do not have the stabilizing electrostatic interactions of the octanol alcohol group, we cannot simulate this behavior. At the moment, not even the titratable water partitions accurately into octanol.

We have verified that our titratable beads in the charged and neutral state do not excessively aggregate or repel each other. However, we have not considered their self- or cross-interaction in detail. Whereas the dendrimer test case indicates that the self-interactions are reasonable, one should be cautious when having high concentrations of titratable beads together in one simulation. For the moment, our pH range is limited to values between 3.0 – 8.0. Of course, this restricts the model to this range, but it might also impose other limits. Currently, there appears to be a problem with the free energies of transfer for some primary amines with pKa values outside our pH range. When combining the single beads with neutral fragments, the free energies of transfer are only accurately reproduced after applying a shift in the interactions. One possible reason is that the proton affinity is set not based on the entire titration curve but only on a very small part of it. Although the membrane affinity for our test compound is not so accurate, the dendrimer protonation states are accurately reproduced. Thus, one can use primary amines but should carefully assess the results. For the future, we will aim at covering the full pH scale as well as optimizing the primary amines further.

Whereas the previous limitations can be overcome or only require some caution in interpreting the results, there is one inherent limitation of the model. That is the size of the water model. Because the water model has a limited size representing four water molecules, it is possible that protons cannot be abstracted or donated to molecules with a too small cavity for the CG water to penetrate.

IV. CONCLUSION

We presented a new approach to constant pH simulations that make use of the Martini model as basis. Our model is distinctly different from other methods in three aspects: (1) it utilizes explicit proton beads and classical potentials to mimic protonation effects. Hence, it profits directly from any performance enhancement of current MD codes and should be transferable between codes; (2) interaction parameters are based on reproducing titration curves and pH dependent distribution coefficients. Thus, it is not simply interpolating between the two extremes of the underlying force field. This offers an easy possibility to fine-tune and improve parameters without redesigning the force field; (3) it is based on a building block approach within which a titratable bead is transferable between many different molecules having the same fragment and pKa. We discussed verifications of our model as well as its current limitations. By reproducing pH dependent free energies of more complex molecules built from our titratable beads, it was verified that the building block approach holds. Thus, arbitrarily large and complex molecules are immediately available by using the normal Martini approach combined with titratable beads. Furthermore, membrane affinities were computed for some molecules to show that our approach can also be used for highly heterogeneous

systems including a lipid bilayer. Further support is given by qualitatively reproducing pKa shifts of oleic acid and passive translocation via protonation. Finally, our model reproduces qualitatively the expansion of the dendrimer poly(propylene imine) (PPI) as well as the associated pKa shift of its different generations. This example demonstrated that our model is also able to pick up collective interactions between titratable groups. We expect that our titratable Martini model opens the way to simulate pH dependent processes in a very efficient way, enabling studies involving large and complex systems or high-throughput assays and providing semi-quantitative data.

V. METHODS

A. CG-models and interactions

All simulations utilized a pre-release of Martini3 for the neutral bead interactions and titratable bead interactions as outlined in the paper. All interaction parameters as well as topology (.itp) files are available at https://cgmartini.nl and the supplementary material. Molecule topology (.itp) files for all molecules were generated following the rules of Martini3. That is, each molecule was designed by grouping on average 4 non-hydrogen atoms into one regular sized bead for linear fragments and 5 heavy atoms for branched fragments. Likewise, small beads are used for 4 non-hydrogen atoms, which are branched, and 3 heavy atoms if they are in a linear chain. The same scheme applied to tiny beads. The type of the neutral beads was assigned based on the fragment free energies of transfer.

B. Titration simulations

All titration simulations were carried out with the GROMACS software (version 2018)[54], using the stochastic dynamics integrator[55] (with inverse friction constant 1.0 ps) and a time step of 8 fs–10 fs. Production runs (with the exception of PPI) were carried out in the NpT ensemble at 298.15 K. Pressure was maintained at 1 bar using the Parinello–Rahman barostat[56] (time constant 12.0 ps and compressibility 4.5×10^{-5} bar^{-1}). Each simulation was simulated for 50 ns. With the exception of the amines with pKa larger than 8, each simulation consisted of a single titratable molecule in a box of about 1900 Martini water beads. For amines with pKa larger than 8, 16 molecules were solvated in the same number of water molecules to enhance sampling. For the simulation of the poly(propylene imine) dendrimer, we utilized Berendsen pressure coupling[57] (time constant 3.0 ps and compressibility 4.5×10^{-5} bar^{-1}). Each simulation was run for 400 ns. At each pH, the dendrimer was solvated in 1936 Martini water molecules. For all simulations, the degree of protonation was determined using a home-made analysis script (https://github.com/fgrunewald/titratable_martini_tools). The script computes the distance of a proton to all titratable beads in a radius of 1.1 nm. If the proton is closer to the titratable bead of interest than to any other bead, the titratable bead of interest is considered to be protonated. If more than one proton is closer, we still count this as protonated. The error and convergence was analyzed utilizing a home-made statistical analysis code as described elsewhere.[6] Fitting of the titration curves was done using the symfit python library.[58]

C. Free energy of transfer

All simulations for free energies of transfer were carried out with the GROMACS software (version 2018),[54] using the stochastic dynamics integrator[55] (with inverse friction constant 1.0 ps) and a time step of 8 fs–10 fs. Free energies of transfer from hexadecane to water for the acid type beads were computed using umbrella sampling.[59] Each simulation consisted of a biphasic hexadecane (HD) water system with 2001 hexadecane molecules and 8000 water molecules. The acid bead was simulated with a distance constraint with respect to the center-of-mass of the HD phase covering the distances from HD to water using a 1 Å spacing between windows. This resulted in 36 windows. Each window was run under NpzA conditions at 1 bar pressure in the z-direction (normal to the HD/water interface) maintained with a Berendsen barostat[57] using a coupling time of 12 ps and compressibility of 3×10^{-4} bar^{-1}. Sampling times per window varied from for 7 ns–50 ns depending on convergence and the size of the molecule. The temperature was maintained at 298.15 K using a v-rescale thermostat with 1 ps. Reweighting of the biased free-energy differences was done using the WHAM algorithm[60] implemented in GROMACS. The free energy of transfer was computed from the PMF profile by taking the error weighted average in water and HD and subsequently subtracting the average. The standard error was propagated accordingly.

Free energies of transfer of base type beads were calculated as differences between free energies of solvation in water and hexadecane. Solvation free energies were computed by alchemical free energy transformations as implemented in the GROMACS package. With the exception of all amines with pKa larger than 10, systems consisted of a single molecule in at least 1900 Martini water beads. The system's composition for the aforementioned amines was the same as in the titration simulations, and 6 of them were coupled at the same time. For the calculations, using titratable water, in total 24 nonequally spaced windows were used, switching first the Coulomb and subsequently LJ interactions. Soft-core LJ potentials were applied following the recommended values.[61] Each window was run under NpT conditions for 10 ns at 1 bar pressure maintained with a the Parinello–Rahman barostat[57] using a coupling time of 4 ps and a compressibility of 4.5×10^{-5} bar^{-1}. Temperature was maintained at 298.15 K. The derivative of the potential energy was recorded every 50 steps. The solvation free energy in hexadecane was computed using the regular Martini3 model with a 20 fs time step, using 14 windows for the LJ part, and calculating the derivative every 10 steps. Pressure coupling and soft-core settings were the same as used before. All the free energies of the transformation were estimated using the Multistate-Bennetts-Acceptance-Ratio (MBAR) method,[62] obtained using a python tool available on Github (https://github.com/davidlmobley/alchemical-analysis). For each calculation, the convergence and quality of the calculations were checked following the guidelines suggested by Klimovich, Shirts, and Mobley.[63] The error reported with the calculations is the statistical error estimate. The intramolecular interactions were not switched off for both sets of simulations.

We used these two different protocols because the neutral acid consists of two charged and, in principle, independent particles. Switching off a neutral acid (i.e., a negative fragment and one proton bead) by alchemical free energy transformation leads to problems with consistency and convergence. This comes in

addition to the problems related to computing accurate solvation free energies of ions as detailed by Hunenberger and Reif.[64] These problems do not occur for bases because the neutral base fragment is a single molecule. Thus, we used the slightly faster alchemical transformation protocol as outlined before for the bases.

D. Fatty acid and small molecule membrane simulations

Fatty acid simulations for the titration and translocation were carried out in a POPC membrane using the default leap-frog integrator. Each simulation was run under NpT conditions using semi-isotropic pressure coupling (Parrinello–Rahman) at 1 bar pressure. The lateral directions were coupled together separately from the normal (z) direction using a coupling time of 12 ps and a compressibility of 3×10^{-4} bar^{-1}. Temperature was maintained at 310 K using the v-rescale thermostat[65] with a coupling time of 1 ps. Each pH window was run for 50 ns. The system for both simulations was composed of 10 fatty acids in 133 POPC lipids per leaflet solvated in a total of 6747 Martini water beads. Free energies of binding of small molecules to a lipid bilayer were computed by integrating the PMFs of binding obtained using adaptive weighted histogram sampling[66] along the bilayer normal direction. Integration was carried out as suggested by Hinner et al.[67] and further described in the supplementary material. The parameters for the small molecules were obtained by mapping the atomistic structure following the Martini3 guidelines and assigning neutral bead types based on the free energy of transfer. Bonded interactions were obtained by mapping atomistic distributions or QM data. Topology files with all parameters are available in the supplementary material. For these simulations, the SD integrator with the same pressure coupling as for the fatty acids was utilized. Each simulation consisted of 169 lipids per leaflet and about 5800 water molecules in total. Temperature and lipid types are reported in Table S7 and correspond to the conditions used in experiments. To obtain an error estimate, we ran three replicates of 800 ns and computed the error from those.

SUPPLEMENTARY MATERIAL

See the supplementary material for additional verifications, topology files, video of proton hopping, and fatty acid flip-flop, individual data points for of free energy of transfer, pKa values and membrane affinities, and in depth explanation of protocol for computing membrane affinities.

ACKNOWLEDGMENTS

DATA AVAILABILITY

The data that support the findings of this study are available from the corresponding author upon reasonable request.

REFERENCES

[1] S. J. Marrink, H. J. Risselada, S. Yefimov, D. P. Tieleman, and A. H. De Vries, J. Phys. Chem. B **111**, 7812 (2007).

[2] H. I. Ingólfsson, M. N. Melo, F. J. Van Eerden, C. Arnarez, C. A. Lopez, T. A. Wassenaar, X. Periole, A. H. De Vries, D. P. Tieleman, and S. J. Marrink, J. Am. Chem. Soc. **136**, 14554 (2014).

[3] F. J. Van Eerden, M. N. Melo, P. W. J. M. Frederix, X. Periole, and S. J. Marrink, Nat. Commun. **8**, 15214 (2017).

[4] L. Monticelli, S. K. Kandasamy, X. Periole, R. G. Larson, D. P. Tieleman, and S.-J. Marrink, J. Chem. Theory Comput. **4**, 819 (2008).

[5] R. Alessandri, J. J. Uusitalo, A. H. de Vries, R. W. A. Havenith, and S. J. Marrink, J. Am. Chem. Soc. **139**, 3697 (2017).

[6] F. Grunewald, G. Rossi, A. H. de Vries, S. J. Marrink, and L. Monticelli, J. Phys. Chem. B **122**, 7436 (2018).

[7] P. W. J. M. Frederix, G. G. Scott, Y. M. Abul-Haija, D. Kalafatovic, C. G. Pappas, N. Javid, N. T. Hunt, R. V. Ulijn, and T. Tuttle, Nat. Chem. **7**, 30 (2015).

[8] Z. Yue, C. Li, G. A. Voth, and J. M. J. Swanson, J. Am. Chem. Soc. **141**, 13421 (2019).

[9] C. Hannesschlaeger, A. Horner, and P. Pohl, Chem. Rev. **119**, 5922 (2019).

[10] H. Watanabe, C. Yoshida, A. Ooishi, Y. Nakai, M. Ueda, Y. Isobe, and S. Honda, ACS Chem. Biol. **14**, 2729 (2019).

[11] M. C. Childers and V. Daggett, Biochemistry **58**, 4408 (2019).

[12] T. M. D. Le, H. T. T. Duong, T. Thambi, V. H. Giang Phan, J. H. Jeong, and D. S. Lee, Biomacromolecules **19**, 3536 (2018).

[13] G. A. Voth, Front. Biosci. **8**, 1213 (2003).

[14] H. L. Tepper and G. A. Voth, Biophys. J. **88**, 3095 (2020).

[15] M. S. Lee, F. R. Salsbury, and C. L. Brooks, Proteins Struct. Funct. Bioinform. **56**, 738 (2004).

[16] S. Donnini, F. Tegeler, G. Groenhof, and H. Grubmüller, J. Chem. Theory Comput. **7**, 1962 (2011).

[17] A. M. Baptista, V. H. Teixeira, and C. M. Soares, J. Chem. Phys. **117**, 4184 (2002).

[18] J. Mongan, D. A. Case, and J. A. McCammon, J. Comput. Chem. **25**, 2038 (2004).

[19] Y. Huang, W. Chen, J. A. Wallace, and J. Shen, J. Chem. Theory Comput. **12**, 5411 (2016).

[20] J. A. Wallace and J. K. Shen, J. Chem. Phys. **137**, 184105 (2012).

[21] W. Chen, J. A. Wallace, Z. Yue, and J. K. Shen, Biophys. J. **105**, L15 (2013).

[22] P. Dobrev, S. Donnini, G. Groenhof, and H. Grubmüller, J. Chem. Theory Comput. **13**, 147 (2017).

[23] S. Donnini, R. T. Ullmann, G. Groenhof, and H. Grubmüller, J. Chem. Theory Comput. **12**, 1040 (2016).

[24] W. F. D. Bennett, A. W. Chen, S. Donnini, G. Groenhof, and D. P. Tieleman, Can. J. Chem. **91**, 839 (2013).

[25] B. K. Radak, C. Chipot, D. Suh, S. Jo, W. Jiang, J. C. Phillips, K. Schulten, and B. Roux, J. Chem. Theory Comput. **13**, 5933 (2017).

[26] S. O. Yesylevskyy, L. V. Schäfer, D. Sengupta, and S. J. Marrink, PLoS Comput. Biol. **6**, e1000810 (2010).

[27] Z. Wu, Q. Cui, and A. Yethiraj, J. Chem. Theory Comput. **7**, 3793 (2011).

[28] J. Michalowsky, L. V. Schäfer, C. Holm, and J. Smiatek, J. Chem. Phys. **146**, 054501 (2017).

[29] N. Agmon, Chem. Phys. Lett. **244**, 456 (1995).

[30] M. Eigen, Angew. Chem., Int. Ed. **3**, 1 (1964).

[31] S. Kim, J. Chen, T. Cheng, A. Gindulyte, J. He, S. He, Q. Li, B. A. Shoemaker, P. A. Thiessen, B. Yu, L. Zaslavsky, J. Zhang, and E. E. Bolton, Nucl. Acids Res. **47**, D1102 (2019).

[32]C. C. Bannan, K. H. Burley, M. Chiu, M. R. Shirts, M. K. Gilson, and D. L. Mobley, J. Comput. Aided Mol. Des. **30**, 927 (2016).

[33]D. H. de Jong, S. Baoukina, H. I. Ingólfsson, and S. J. Marrink, Comput. Phys. Commun. **199**, 1 (2016).

[34]S. T. J. Droge, J. L. M. Hermens, J. Rabone, S. Gutsell, and G. Hodges, Environ. Sci. Process. Impacts **18**, 1011 (2016).

[35]H. K. Hall, J. Am. Chem. Soc. **79**, 5441 (1957).

[36]S. Spycher, P. Smejtek, T. I. Netzeva, and B. I. Escher, Chem. Res. Toxicol. **21**, 911 (2008).

[37]W. Zhang and A. C. T. Van Duin, J. Phys. Chem. B **121**, 6021 (2017).

[38]T. S. Light, S. Licht, A. C. Bevilacqua, and K. R. Morash, Electrochem. Solid-State Lett. **8**, E16 (2005).

[39]M. H. Abraham, H. S. Chadha, G. S. Whiting, and R. C. Mitchell, J. Pharm. Sci. **83**, 1085 (1994).

[40]S. Natesan, Z. Wang, V. Lukacova, M. Peng, R. Subramaniam, S. Lynch, and S. Balaz, J. Chem. Inf. Model. **53**, 1424 (2013).

[41]A. Leo, C. Hansch, and D. Elkins, Chem. Rev. **71**, 525 (1971).

[42]A. Avdeef, K. J. Box, J. E. A. Comer, C. Hibbert, and K. Y. Tam, Pharm. Res. **15**, 209 (1998).

[43]K. Bittermann, S. Spycher, S. Endo, L. Pohler, U. Huniar, K.-U. Goss, and A. Klamt, J. Phys. Chem. B **118**, 14833 (2014).

[44]R. M. Peitzsch and S. McLaughlin, Biochemistry **32**, 10436 (1993).

[45]P. Høyrup, J. Davidsen, and K. Jørgensen, J. Phys. Chem. B **105**, 2649 (2001).

[46]A. A. Pashkovskaya, M. Vazdar, L. Zimmermann, O. Jovanovic, P. Pohl, and E. E. Pohl, Biophys. J. **114**, 2142 (2018).

[47]M. Ptak, M. Egret-Charlier, A. Sanson, and O. Bouloussa, Biochim. Biophys. Acta - Biomembr. **600**, 387 (1980).

[48]B. H. Morrow, P. H. Koenig, and J. K. Shen, J. Chem. Phys. **137**, 194902 (2012).

[49]F. Kamp and J. A. Hamilton, Proc. Natl. Acad. Sci. U. S. A. **89**, 11367 (1992).

[50]K. Brunaldi, M. A. Miranda, F. Abdulkader, R. Curi, and J. Procopio, J. Lipid Res. **46**, 245 (2005).

[51]M. C. Ramos, V. A. C. Horta, and B. A. C. Horta, J. Chem. Inf. Model. **59**, 1444 (2019).

[52]R. C. Van Duijvenbode, M. Borkovec, and G. J. M. Koper, Polymer **39**, 2657 (1998).

[53]P. B. P. S. Reis, D. Vila-vic, S. R. R. Campos, A. M. Baptista, and M. Machuqueiro, ACS Omega **3**, 2001 (2018).

[54]M. J. Abraham, T. Murtola, R. Schulz, S. Páll, J. C. Smith, B. Hess, and E. Lindahl, SoftwareX **1-2**, 19 (2015).

[55]N. Goga, A. J. Rzepiela, A. H. de Vries, S. J. Marrink, and H. J. C. Berendsen, J. Chem. Theory Comput. **8**, 3637 (2012).

[56]M. Parrinello and A. Rahman, J. Appl. Phys. **52**, 7182 (1981).

[57]H. J. C. Berendsen, J. P. M. Postma, W. F. van Gunsteren, A. DiNola, and J. R. Haak, J. Chem. Phys. **81**, 3684 (1984).

[58]M. Roelfs and P. C. Kroon, symfit, tBuLi/symfit: symfit 0.5.2 (Version 0.5.2), Zenodo. http://doi.org/10.5281/zenodo.3532953.

[59]J. Kästner, Wiley Interdisc. Rev. Comput. Mol. Sci. **1**, 932 (2011).

[60]S. Kumar, J. M. Rosenberg, D. Bouzida, R. H. Swendsen, and P. A. Kollman, J. Comput. Chem. **13**, 1011 (1992).

[61]M. R. Shirts and D. L. Mobley, "An introduction to best practices in free energy calculations," in *Biomolecular Simulations. Methods in Molecular Biology (Methods and Protocols)* (Humana Press, Totowa, NJ, 2013), Vol. 924, pp. 271–311.

[62]M. R. Shirts and J. D. Chodera, J. Chem. Phys. **129**, 124105 (2008).

[63]P. V. Klimovich, M. R. Shirts, and D. L. Mobley, J. Comput. Aided. Mol. Des. **29**, 397 (2015).

[64]P. Hünenberger and M. Reif, *Single-Ion Solvation* (Royal Society of Chemistry, Cambridge, 2011).

[65]G. Bussi, D. Donadio, and M. Parrinello, J. Chem. Phys. **126**, 014101 (2007).

[66]V. Lindahl, J. Lidmar, and B. Hess, J. Chem. Phys. **141**, 044110 (2014).

[67]M. J. Hinner, S.-J. Marrink, and A. H. De Vries, J. Phys. Chem. B **113**, 15807 (2009).